Investigation of the validity of radiosity for sound-field prediction in cubic rooms

Eva-Marie Nosal[a)]
Department of Mathematics, University of British Columbia, 1984 Mathematics Road, Vancouver, BC, V6T 1Z2 Canada

Murray Hodgson
School of Occupational and Environmental Hygiene and Department of Mechanical Engineering, University of British Columbia, 2206 East Mall, Vancouver, BC, V6T 1Z3 Canada

Ian Ashdown
Heart Consultants Limited, 620 Ballantree Road, West Vancouver, BC, V7S 1W3 Canada

(Received 3 October 2003; revised 2 June 2004; accepted 12 September 2004)

This paper explores acoustical (or time-dependent) radiosity using predictions made in four cubic enclosures. The methods and algorithms used are those presented in a previous paper by the same authors [Nosal, Hodgson, and Ashdown, J. Acoust. Soc. Am. **116**(2), 970–980 (2004)]. First, the algorithm, methods, and conditions for convergence are investigated by comparison of numerous predictions for the four cubic enclosures. Here, variables and parameters used in the predictions are varied to explore the effect of absorption distribution, the necessary conditions for convergence of the numerical solution to the analytical solution, form-factor prediction methods, and the computational requirements. The predictions are also used to investigate the effect of absorption distribution on sound fields in cubic enclosures with diffusely reflecting boundaries. Acoustical radiosity is then compared to predictions made in the four enclosures by a ray-tracing model that can account for diffuse reflection. Comparisons are made of echograms, room-acoustical parameters, and discretized echograms. © *2004 Acoustical Society of America.* [DOI: 10.1121/1.1811473]

PACS numbers: 43.55.Ka, 43.55.Br [MK] Pages: 3505–3514

I. INTRODUCTION

In the initial phase[1] of the current research, algorithms and methods were developed for acoustical radiosity for arbitrary polyhedral enclosures, based on a numerical solution to the integral equation. These were programed in MATLAB (Ref. 2) and validated by comparison to analytical solutions for a spherical enclosure.

Further research is required to understand the necessary and sufficient conditions for convergence of the solution found by the algorithms and methods to the analytical solution. The numerical solution has been applied several times in the literature[3–7] but, apart from Schroeder and Hackman's[8] investigations for a two-dimensional enclosure, there has been little or no systematic investigation of the effect of various prediction parameters, such as the space and time resolutions. Questions that need to be addressed include: how many patches and/or elements are needed?; what time resolution is fine enough?; how far (in time) does the prediction need to be made?; what part of this should be exact (without the averaging outlined in Nosal *et al.*[1])?; and, what is the error introduced by the use of configuration factors to approximate form factors[1]? This research explores acoustical radiosity thoroughly for one case—that of a cubic enclosure—and leads to a better understanding of the factors involved in acoustical radiosity predictions.

Similarly, little effort has previously been put into the comparison of acoustical radiosity to other prediction methods. Work by Le Bot and Bocquillet,[9] in which radiosity and ray tracing are compared, focuses only on steady-state sound-pressure levels. Further comparison of the two prediction techniques is another objective of this research. To do so, predictions are made for the four cubic enclosures using RAYCUB, a ray-tracing model that can account for diffuse reflection, and are compared to the predictions made by acoustical radiosity. Acoustical radiosity and ray tracing with diffuse reflection are expected to give identical predictions in limiting cases.[9]

II. PARAMETERS, ECHOGRAMS, AND DISCRETIZED ECHOGRAMS

Listener perception of a sound field is affected by two main attributes of the field. The first is the arrival time and strength of the direct signal and the first-order reflections. Differences between sound fields with respect to these reflections can be seen by comparing echograms—perhaps the most fundamental and detailed method of comparison. This comparison reveals information about the prominent reflections and other fine details about the distribution of energy in time.

The other perceptible attribute of the field is the temporal distribution of energy. It is difficult to get information about this distribution by comparison of echograms, so other

[a)]Current affiliation: School of Ocean and Earth Sciences and Technology, Department of Geology and Geophysics, University of Hawaii at Manoa, 1680 East-West Road POST 813, Honolulu, HI, 96822. Electronic mail: nosal@hawaii.edu

TABLE I. Distribution of absorption in the cubic rooms. In all cases, $\bar{\alpha} = 1/6$.

Cube	Distribution of absorption
1	$\alpha = \frac{1}{6}$ over all walls
2	$\alpha = 1$ on the floor, 0 on the other walls
3	$\alpha = \frac{1}{2}$ on the floor and the ceiling, 0 on the other walls
4	$\alpha = \frac{1}{2}$ on the floor and the front wall, 0 on the other walls

methods of comparison must be used. One method is to compare room-acoustical parameters, most of which are measures of energy distribution (for example, clarity and definition[10] are defined by ratios of early and late energies). Parameters used for comparisons in this paper are sound-pressure level (L_p), center time (TS), early decay time (EDT), reverberation time (RT), clarity (C_{80}), and definition (D_{50}).[10] They have been well correlated with listener perception.[11] Nevertheless, much information about the exact distribution of energy is lost to the parameters, since they are not highly sensitive to subtle changes in energy distribution.

To enable comparison of such changes, ''echogram discretization'' is used in this research as a way to compare total energy levels within small time steps. The idea is very simple: time is discretized, and all energy arriving between points of discretization is summed to give the total energy for the corresponding time step (a similar method of comparison has previously been used by Suh *et al.*[12]). Obviously, the resolution used in the echogram discretization must be coarser than the time resolution used in the radiosity algorithm (or, in the case of measurements, the inverse of the sampling frequency). Note that using a longer time interval in the radiosity algorithm is not equivalent to using a small time interval in radiosity and then using the longer interval in the discretization of the echogram. We have chosen to use discretized echograms with 50-ms time steps. The resolution is somewhat arbitrary (not corresponding to perceptual issues or otherwise), and was chosen since it provided a substantial, but not overwhelming, amount of information. In the cases considered, the use of smaller or larger time steps gave similar results and led to similar conclusions.

III. RADIOSITY PREDICTIONS

A. Preliminary remarks

The radiosity algorithm was run numerous times for four cubic rooms. Each cube had walls 8 m long, and an average absorption coefficient of 1/6. The absorption was distributed as indicated in Table I.

Predictions were made, varying: (1) the number of patches (only a single-level hierarchy was applied); (2) the resolution of the time discretization; (3) the length of time for which exact and approximate predictions are made; and (4) the form-factor prediction method. The effect of the varying distribution of absorption (among the four cubes) was investigated using the results, and comparisons were made with predictions by ray tracing. For each prediction, the source was at the center of the cube and had power of 0.005 W. The receiver was located inside the enclosure 2 m from the floor, the front wall, and a sidewall, respectively (by symmetry of the configurations, which sidewall does not matter). Air absorption was neglected throughout—in the way that it is incorporated, it has no effect on convergence.

B. Patch size

1. Specifications

The numerical solution is based on a discretization of the boundary. This results in discretization error, which should be reduced as the resolution of the meshing is increased. In particular, as the resolution increases, the numerical solution approaches the analytical solution. To minimize computational requirements, it is desirable to minimize the number of patches used in the discretization.

For each cube, the radiosity algorithm was run ten times with an increasing number of patches. The first prediction for each cube had each wall as a single patch, giving a total of six patches. For the second prediction, each wall was divided into four equally sized, rectangular patches, giving 24 patches in total. The third prediction had nine patches on each wall for a total of 54 patches, the fourth had 16 giving 96 in total, and so on (in general, the nth prediction had n^2 patches on each wall and $6n^2$ patches in total).

The predictions were made with a discretization period of $\Delta t = 1/24\,000$ s. This was chosen based on initial predictions that indicated that there is almost no variation in room-acoustical parameter predictions if time is discretized more finely than $\Delta t = 1/18\,000$ s. Form factors were found using the analytical formulas given by Gross *et al.*[13]

In the methods used here,[1] predictions are made using the exact radiosity algorithm for time steps up to t_{exact}. For time steps between t_{exact} and t_{final}, which is the last time step for which predictions are made, radiation densities are estimated using an averaging technique.[1]

t_{exact} and t_{final} were set to 0.8 and 1.0 s, respectively, based on a criterion developed by Nosal.[14] The criterion guarantees that the reverberation time predicted from the truncated impulse response is within ϵ of the reverberation time that would be obtained from the full impulse response, provided that truncation of the full impulse response occurs at a time greater than $t_{\min}(\epsilon, \text{RT})$, where

$$t_{\min}(\epsilon, \text{RT}) = \frac{\text{RT}}{6\ln(10)} \times \ln\left[1 + \frac{(10^{-3}e^{[3\ln(10)\epsilon]/\text{RT}}) - 1}{10^{-35/10} - 10^{-5/10}(10^{-3}e^{[3\ln(10)\epsilon]/\text{RT}})}\right], \quad (1)$$

where RT is the reverberation time for the full response.

To apply the criterion, exponential decay was assumed. Miles[6] showed that, in general, the decay curves predicted using the integral equation are strictly exponential after some time. Consequently, even though the first part of the sound decay is not exponential, the assumption of exponential decay along the entire curve may not be unreasonable in this application. Then, according to Eying's classical formula for reverberation time[10]

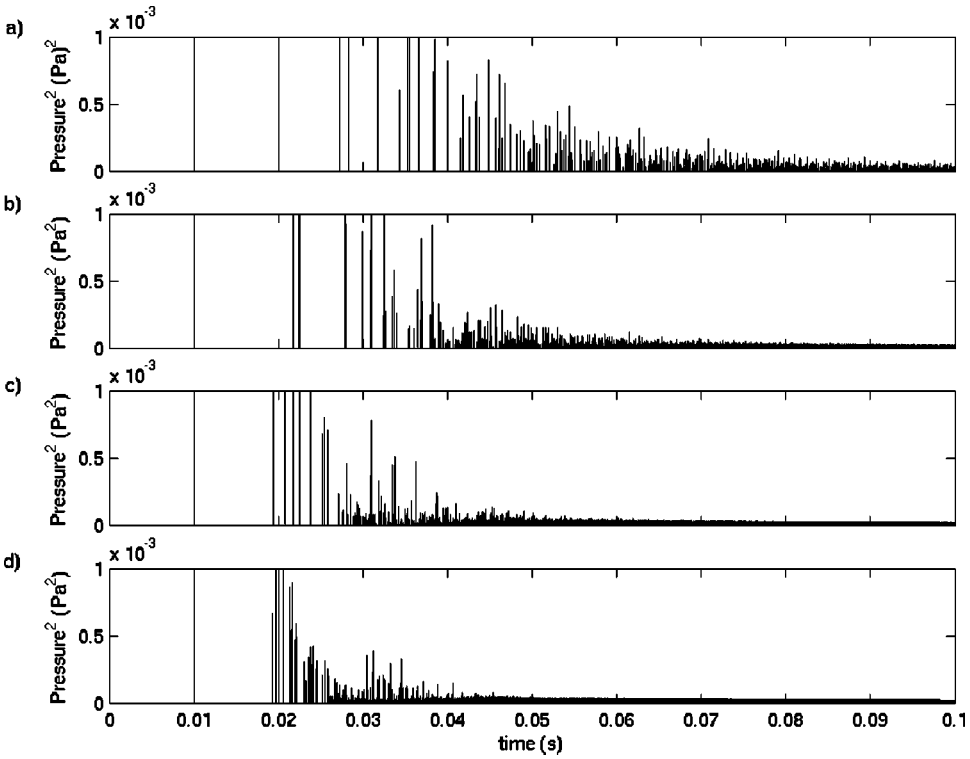


FIG. 1. Echograms for cube 1 from radiosity predictions with (a) 24; (b) 54; (c) 150; and (d) 600 patches ($\Delta t = 1/24\,000$, $t_{\text{exact}} = 0.8$ s, and $t_{\text{final}} = 1.0$ s).

$$\text{RT} = \frac{24V\ln(10)}{c(4mV - S\ln(1-\overline{\alpha}))} \approx 0.161\frac{V}{4mV - S\ln(1-\overline{\alpha})}. \quad (2)$$

The RTs in the cubic rooms should be 1.1782 s [in Eq. (2), V, S, and $\overline{\alpha}$ are room volume, surface area, and average absorption coefficient, respectively, c is the speed of sound, and m is the air absorption coefficient]. Although this reverberation time may not be perfectly accurate (due to the limiting diffuse-field assumption made by Eyring[15]), it can be taken as an initial estimate for use in Eq. (1). If it is desired to predict RT to within 0.01 s of the full impulse response RT (which represents very high accuracy) then, according to this equation, the required t_{final} is given by

$$t_{\text{final}} \geqslant t_{\min}(0.01, 1.1782) = 0.9264 \text{ s}. \quad (3)$$

$t_{\text{final}} = 1.0$ was chosen correspondingly, and t_{exact} was chosen to be quite close to t_{final} (since the effects of varying t_{exact} were unknown).

2. Convergence

Figure 1 shows the echograms for cube 1 obtained from predictions with 24, 54, 150, and 600 patches, respectively. As the meshing is refined, the energy arriving at the receiver is spread out in time, with fewer distinct reflections. Indeed, the echogram for 600 patches has none of the prominent, large peaks that the echogram for 24 patches has (apart from the direct signal). An explanation for this observation is that, with a finer meshing, the energy leaving a patch is divided into more parts to propagate to the other patches, so that large units of energy are quickly dissipated. This is what is expected in a room with diffusely reflecting boundaries.

In a real room, with partially specularly reflecting boundaries, some distinct reflections would be expected, suggesting that fewer patches may yield echograms that look more similar to measured echograms. However, this should not be interpreted as meaning that predictions with fewer patches yield more realistic predictions. The arrival times and amplitudes of the distinct reflections in such predictions are unrealistic and do not correspond to times and amplitudes that would result from specular reflection.

Figure 2 shows a discretized echogram for cube 1 with time intervals of 0.05 s. For each time interval, the pressure-squared sums for predictions with 6, 54, 150, and 600 patches, respectively, are plotted. From the graphs, it is evident that more patches tend to result in more energy in the very early time steps, with levels becoming more uniform at about 0.15 s. This trend reverses itself from about 0.2 to 0.35 s, after which energy levels are very similar. The most noticeable changes in the echograms and discretized echograms occur for predictions with less than 150 patches. For more than 150 patches, there is less change, with predictions for 150 patches similar to those for 600 patches. This indicates that 150 patches are sufficient for accurate predictions.

In Table II, the predicted values of the various parameters are given for varying numbers of patches. These values are for cube 1; the trends are very similar for all four cubes. Each of the parameters considered (L_p, C_{80}, D_{50}, EDT, RT, and TS) converges to a finite value as the number of patches increases. The percent difference between consecutive predictions decreases with increasing number of patches [here, consecutive means between the nth and the $(n+1)$th prediction, with $6n^2$ and $6(n+1)^2$ patches, respectively]. This suggests convergence by the ratio test.[16] The validation of the numerical solution for the sphere[1] provides confidence that the numerical solution does indeed converge (with increasing number of patches) to the analytical solution to the integral equation.

C_{80} is the slowest to converge of all the parameters.

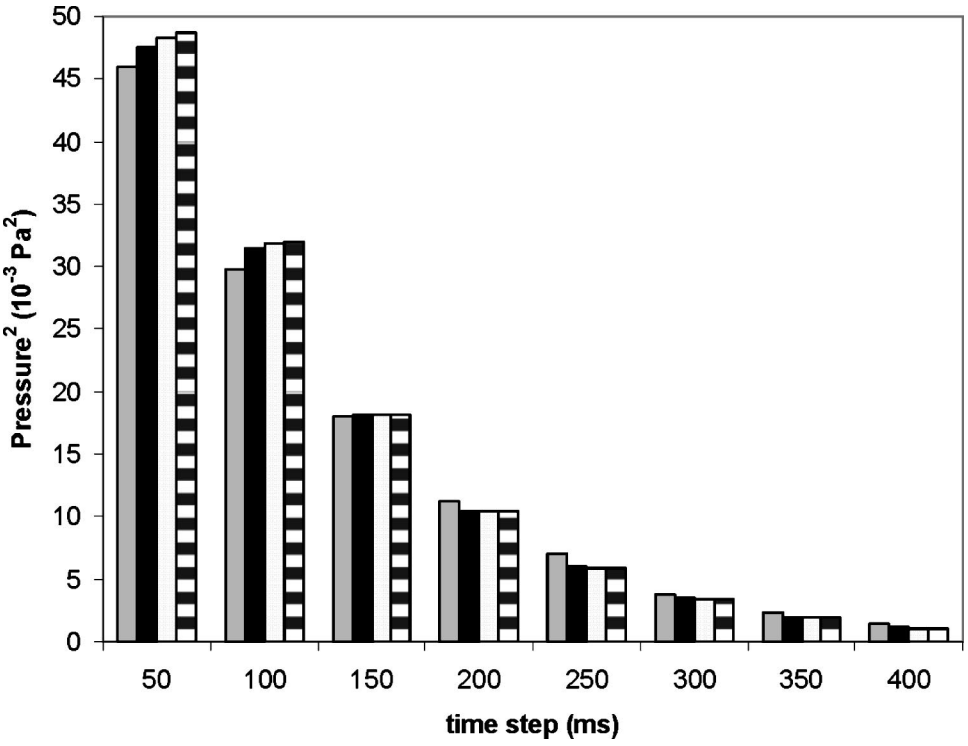


FIG. 2. Discretized echogram for cube 1 with 6 patches; 54 patches; 150 patches; 600 patches ($\Delta t = 1/24\,000$, $t_{\text{exact}} = 0.8$ s, and $t_{\text{final}} = 1.0$ s).

However, even in the case where it is slowest to converge (cube 1), the differences between the fifth and sixth predictions of C_{80} are less than 1%. In fact, all of the other parameters (in all cubes) have differences less than 1% between the third and fourth predictions. Indeed, a fine subdivision of the enclosure is not necessary in these trials, and 150 patches are sufficient for good predictions, as in the echograms. Worth noting is that the differences between the L_p's for the first and second prediction is less than 1% (in all cubes). This suggests that (in a cubic room) radiosity can be used with a very coarse subdivision (one patch per wall in this case) to predict steady-state sound-pressure levels in rooms with diffusely reflecting boundaries, even with nonuniformly distributed absorption.

It is important to realize that required patch size does not depend on the frequency of the sound that is being considered. This is due to the fact that phase is not accounted for in radiosity. Indeed, the integral equation is the same for any frequency, except for the values of absorption coefficients and air absorption exponents; consequently, convergence of the numerical solution to the analytical solution is not frequency dependent (apart from changes in convergence with varying absorption). Convergence of the numerical solution to the analytical solution is not to be confused with convergence to the true solution (the solution that would be obtained in a real room). It is possible that the analytical solution to the integral equation (which is the converged numerical solution) is closer to the true solution at higher frequencies, because phase effects are less significant at these frequencies. The phase independence of radiosity might also help to explain the adequacy of a coarse subdivision of the enclosure surfaces. Still, it is important to keep the relationship between patch size and the wavelength of sound being considered in mind when working with acoustical radiosity.

TABLE II. Parameter predictions with varying number of patches for cube 1 ($\Delta t = 1/24\,000$, $t_{\text{exact}} = 0.8$ s, and $t_{\text{final}} = 1.0$ s).

Number of patches	L_p (dB)	C_{80} (dB)	D_{50} (%)	EDT (s)	RT (s)	TS (ms)
6	84.83	1.60	43.29	1.35	1.42	102.93
24	84.82	1.85	45.04	1.27	1.23	97.16
54	84.83	1.92	45.43	1.24	1.21	95.95
96	84.85	2.97	45.74	1.23	1.20	95.02
150	84.86	2.00	45.87	1.23	1.20	94.67
216	84.86	2.02	46.98	1.22	1.19	94.42
294	84.86	2.04	46.04	1.22	1.19	94.28
384	84.86	2.05	46.14	1.22	1.19	94.17
486	84.87	2.06	46.18	1.22	1.19	94.11
600	84.87	2.06	46.20	1.22	1.19	94.07

3. Absorption distribution

It is of interest to use predictions made for the four different cubes to investigate the effect of different distributions of absorption. As mentioned above, the average absorption coefficient in each cube was 1/6. Refer to Table III for the predicted parameters (from the run with 150 patches).

RT is longest in cube 1, with uniform absorption, and shortest in cube 2, which has absorption on the floor. The

TABLE III. Parameter predictions for the four cubic rooms (150 patches, $\Delta t = 1/24\,000$, $t_{\text{exact}} = 0.8$ s, and $t_{\text{final}} = 1.0$ s).

Cube	L_p (dB)	C_{80} (dB)	D_{50} (%)	EDT (s)	RT (s)	TS (ms)
1	84.86	2.00	45.87	1.23	1.20	94.67
2	84.99	2.85	49.88	1.08	1.06	84.5
3	84.63	2.39	47.83	1.17	1.16	89.7
4	84.67	2.35	47.58	1.17	1.16	90.2

13% difference in RT in these cubes indicates that absorption distribution has a significant effect on RT. Following a line of reasoning set forward by Schroeder and Hackman,[8] cube 2 has the lowest RT because the absorbent surface ''sees'' only reflective surfaces. In the other cubes, the absorbing surfaces see surfaces that absorb some of the sound, so they receive lower sound energy than they would from reflecting surfaces. In cube 1, no surfaces are fully reflecting, so that absorbing surfaces see only other absorbing surfaces, resulting in a lower decay rate and higher RT. Since the absorbing surfaces in cubes 3 and 4 see both reflecting and absorbing surfaces, the RTs are between those in cube 1 and cube 4.

L_p's are very similar (within 0.4 dB) for all four enclosures. Predicted values of C_{80} and D_{50}, which are lower for cube 1 and higher for cube 4, are consistent with the predictions of RT. For higher RTs, lower C_{80} and D_{50} values are expected, because a slower decay rate means more late energy, giving lower early-to-late energy ratios. Similarly, higher and lower TSs for cubes 1 and 4, respectively, are consistent with the RT results.

4. Computational efficiency

Experimental data suggest that radiosity, in a single-level hierarchy, is associated with a computational time complexity of order n^2, where n is the number of patches. This can be explained theoretically as follows. At each time step, and for each element, $(n-1)$ elements must be considered in the calculations. Since there are n elements in total, this gives $n\cdot(n-1)$ calculations for each time step, giving a time complexity of order n^2. For a two-level hierarchy with n elements and m patches, we expect a complexity of order $m\cdot n$.

Also suggested by experimental data is a memory complexity of order n; the memory requirement increases linearly with the number of patches. Once again, this makes sense theoretically because, for each element, radiation densities must be computed for all time steps, so that there are always $n\cdot$(number of time steps) values to be stored.

Refer to Fig. 3 for plots of elapsed time versus number of patches, and for memory requirement versus number of patches. The run times and memory requirements are for predictions for cube 2 (and are similar for the other cubes). A Pentium IV 2.2-GHz PC was used for these predictions.

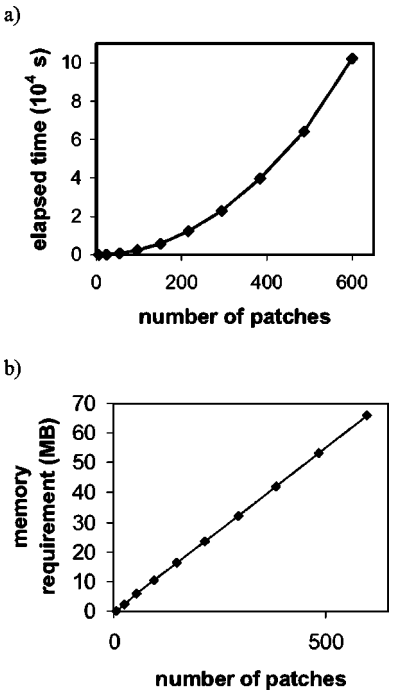


FIG. 3. Variation of (a) elapsed time; and (b) memory requirement with number of patches for cube 2 ($\Delta t = 1/24\,000$, $t_{\text{exact}} = 0.8$ s, and $t_{\text{final}} = 1.0$ s).

C. Time resolution

First, it should be recognized that the nature of time resolution in the radiosity algorithm is quite different from sampling periods used in digital systems and in experimentation. The radiosity algorithm does not simply sample the response every Δt seconds, where Δt is the discretization period. Rather, energy within a time interval is summed to give the energy level for the corresponding time step. Also, phase is neglected in radiosity, so signal frequency does not affect the algorithm (as discussed above). Previous authors have referred to Nyquist's and Shannon's theorems, claiming that, by these theorems, a discretization frequency $(1/\Delta t)$ of at least twice the maximum signal frequency is sufficient. Because it is not clear if the application of these theorems is appropriate, they are not used here.

On the other hand, the Courant number criterion is applicable here. The Courant number[17] can be expressed as $c\Delta t/\Delta x_{\min}$, where $\Delta x_{\min}$ is the minimum distance between patches. To satisfy the Courant number criterion, this number must be less than 1; if the Courant number is too large, then the time resolution must be refined to satisfy the criterion. This ensures that the distance traveled in one time step is not more than the distance between patches. In all investigations performed in this research, the Courant number criterion is satisfied by default (time resolution is fine enough).

To investigate the effect of resolution, further predictions were made for all cubes, with discretization periods of $\Delta t = 1/16\,000$, $1/12\,000$, 1/8000/, 1/4000, 1/2000, and 1/1000 s (recall that the initial predictions had $\Delta t = 1/24\,000$). For these predictions, 600 patches were used to mesh the cubes. Once again, t_{exact} and t_{final} were set to 0.8 and 1.0 s, respectively.

Several echograms for cube 1 are given in Fig. 4. Echograms for the different resolutions look quite similar. Already for $\Delta t = 1/2000$, the distinct early signals are in the same place, and of the same amplitude, as the ones for $\Delta t = 1/24\,000$. The overall amplitudes of the signals in the later parts of the echogram are lower for a finer time resolution, as expected—smaller time steps result in more time steps, each with less energy. From this, it might be concluded that discretization periods of $\Delta t = 1/4000$ are sufficient, and that already at $\Delta t = 1/2000$, reasonable results are obtained.

Discretized echograms for the different time resolutions are almost identical. There tends to be slightly more energy in the early time steps for finer resolutions. This tendency

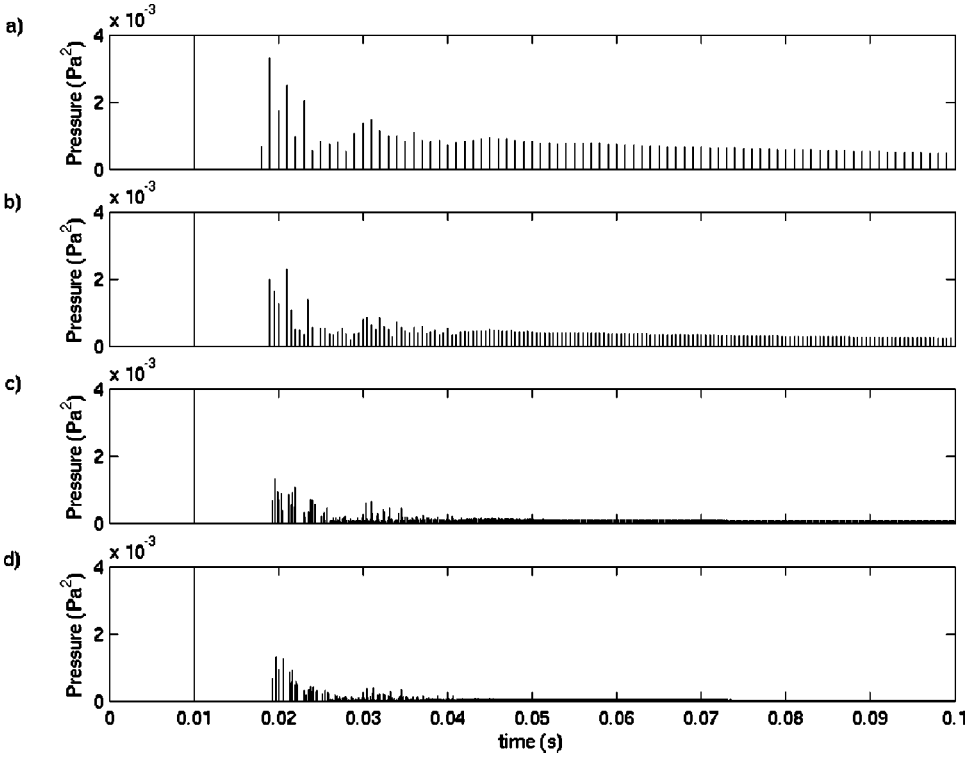


FIG. 4. Echograms for cube 1 with four time resolutions Δt: (a) $\Delta t = 1/1000$ s; (b) $\Delta t = 1/2000$ s; (c) $\Delta t = 1/8000$ s; (d) $\Delta t = 1/24\,000$ s (600 patches, $t_{\text{exact}} = 0.8$ s, and $t_{\text{final}} = 1.0$ s, range reduced to cut off the direct signal, which is the same for all predictions).

reverses for later time steps (after about 0.2 s). Interestingly, this is a similar trend to that for varying patch discretization. Nevertheless, the differences for the varying time resolutions are, for all practical purposes, negligible.

Values for the various parameters versus $1/\Delta t$ are given in Table IV. The values are for cube 4, which has the most significant differences in parameters for different resolutions. Trends for the other cubes are very similar. As is the case for varying patch sizes, the parameter predictions converge with finer resolution. L_p is unaffected by discretization period. This is expected, because different time resolutions do not alter the total energy in the system; they only distribute it differently in time. Values of C_{80}, D_{50}, and TS change minimally for the different discretizations (differences between predictions with $\Delta t = 1/1000$ and $\Delta t = 1/24\,000$ are less than 1%). The most significant changes are for EDT and RT. Even for these parameters, however, predictions for $\Delta t = 1/2000$ are within 1% of predictions for $\Delta t = 1/4000$, and the differences for predictions for $\Delta t = 1/4000$ and $\Delta t = 1/24\,000$ are less than 1%. As with the echograms, this suggests that discretization periods of $\Delta t = 1/4000$ are sufficient for accurate predictions.

TABLE IV. Parameter predictions with varying $1/\Delta t$ for cube 4 (150 patches, $t_{\text{exact}} = 0.8$ s, and $t_{\text{final}} = 1.0$ s).

$1/\Delta t$ (s^{-1})	L_p (dB)	C_{80} (dB)	D_{50} (%)	EDT (s)	RT (s)	TS (ms)
1 000	84.67	2.31	47.86	1.20	1.20	91.21
2 000	84.67	2.32	47.66	1.19	1.19	90.69
4 000	84.67	2.33	47.57	1.18	1.18	90.45
8 000	84.67	2.33	47.53	1.18	1.17	90.30
12 000	84.67	2.35	47.62	1.18	1.16	90.20
16 000	84.67	2.35	47.58	1.17	1.16	90.20
24 000	84.67	2.35	47.58	1.17	1.16	90.20

Both time complexity and memory requirements are of the order $1/\Delta t$, as expected. Figure 5 shows elapsed time versus $1/\Delta t$, and memory requirement versus $1/\Delta t$, for the predictions for cube 1. Once again, the computer was a Pentium IV 2.2-GHz PC.

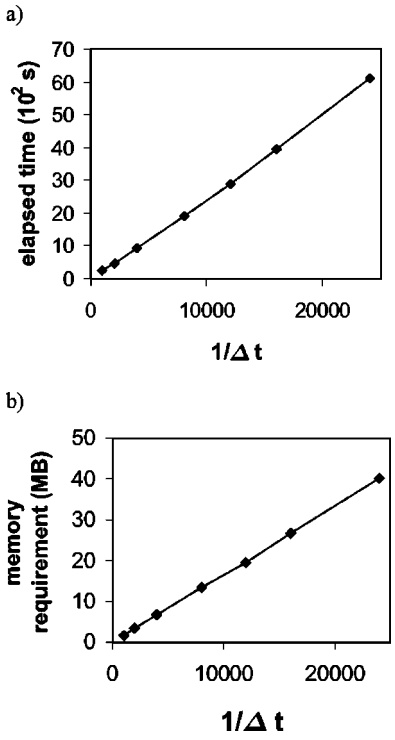


FIG. 5. Variation of (a) elapsed time; and (b) memory requirement with discretization frequency $1/\Delta t$ for cube 1 (150 patches, $t_{\text{exact}} = 0.8$ s, and $t_{\text{final}} = 1.0$ s).

TABLE V. Parameter predictions with varying t_{exact} (s) for cube 1 (t_{final} = 2 s, 150 patches, $\Delta t = 1/12\,000$).

t_{exact} (s)	L_p (dB)	C_{80} (dB)	D_{50} (%)	EDT (s)	RT (s)	TS (ms)
0.05	84.85	1.88	45.89	1.21	1.16	93.75
0.1	84.85	2.00	45.88	1.22	1.16	94.13
0.2	84.86	2.00	45.87	1.23	1.17	94.49
0.3	84.86	2.00	45.87	1.23	1.18	94.61
0.4	84.86	2.00	45.87	1.23	1.19	94.65
0.6	84.86	2.00	45.87	1.23	1.20	94.67
0.8	84.86	2.00	45.87	1.23	1.20	94.67
1.0	84.86	2.00	45.87	1.23	1.20	94.69
1.2	84.86	2.00	45.87	1.23	1.21	94.69
1.4	84.86	2.00	45.87	1.23	1.21	94.69

D. Time limits

It was shown [Eq. (3)] that, to get accurate predictions of RT, the impulse response must be predicted to at least $t_{final} = 0.93$ s. Although this gives an idea of what value of t_{final} to use in predictions, it is still not known what time t_{exact} is required. It is also of interest to investigate the effect of changing t_{final} in the predictions to verify that $t_{final_{min}} = 0.93$ s. To do so, predictions were made for the cubes, with varying t_{final} and t_{exact}. In this investigation, 150 patches were used with $\Delta t = 1/12\,000$.

First, as an ''exact'' case, a prediction was made using $t_{final} = 2$ s and $t_{exact} = 1.4$ s. This was confirmed as the limit to which predictions converge with increasing time limits; there was no change (up to four decimal places) in parameter predictions between this case and predictions with $t_{final} > 2$ s and/or $t_{exact} > 1.4$ s.

For the first set of predictions, t_{final} was held constant at 2 s while t_{exact} was varied (between 0.05 and 1.4 s). In Table V, the parameter predictions for cube 1 are given for varying t_{exact}. From these predictions, it is clear that RT is the parameter most sensitive to changes in t_{exact}. Still, in all cubes, the RT prediction with $t_{exact} = 0.6$ s is different from the exact answer by less than 1%. For all other parameters, $t_{exact} = 0.1$ s is sufficient for the same accuracy (at this exact time limit, RT predictions differ by less that 5%).

To investigate the effect of t_{final}, another set of predictions held t_{exact} constant and varied t_{final}. Table VI gives predictions of the parameters with $t_{exact} = 0.6$ s and varying t_{final}. Predictions do not change significantly as t_{final} is increased beyond 1 s. This is consistent with Eq. (1). Indeed, the prediction with $t_{exact} = 0.6$ s and $t_{final} = 1.0$ s puts all parameter predictions within 1% of the values for the exact case, for all cubes.

TABLE VI. Parameters predictions with varying t_{final} (s) for cube 1 (t_{exact} = 0.6 s, 150 patches, $\Delta t = 1/12\,000$).

t_{final} (s)	L_p (dB)	C_{80} (dB)	D_{50} (%)	EDT (s)	RT (s)	TS (ms)
0.7	84.85	2.00	45.92	1.23	1.16	94.46
0.8	84.86	2.00	45.91	1.23	1.19	94.60
0.9	84.86	2.00	45.91	1.23	1.20	94.66
1.0	84.86	2.00	45.91	1.23	1.20	94.69
1.1	84.86	2.00	45.91	1.23	1.20	94.69
1.2	84.86	2.00	45.90	1.23	1.20	94.69
1.3	84.86	2.00	45.90	1.23	1.20	94.69
1.5	84.86	2.00	45.90	1.23	1.21	94.69
1.6	84.86	2.00	45.90	1.23	1.21	94.69

E. Form factors

As outlined in Nosal *et al.*,[1] HELIOSFF (Ref. 18) was used to find form factors for arbitrary polyhedral rooms. HELIOSFF approximates the form factors by configuration factors; integrals are taken from one point on a patch, rather than from all points on the patch, to the second patch. For this reason, it is necessary to check that the use of these form factors does not significantly affect predictions. To do so, predictions were made for all four cubes under the same conditions as those outlined in Sec. B, using form factors given by HELIOSFF instead of the analytical values. In all cases, the parameters other than C_{80} are within 1% of those found using analytical form factors (in Sec. B) for the meshing with 96 patches. C_{80} is within 1% of the analytical form factor predictions for 150 patches. Echograms and discretized echograms are also very similar to those predicted in Sec. B. It was concluded that approximations made in the determination of form factors by HELIOSFF do not significantly affect predictions, particularly when a reasonably fine (150 patches or more, in this case) meshing of the enclosure is used.

IV. RAY TRACING

A. Diffuse ray tracing with RAYCUB

Having established some understanding of, and confidence in, the acoustical radiosity prediction results for the cubic enclosures, predictions can be compared to ray-tracing predictions for the case of diffuse surface reflection, as assumed by radiosity. The ray-tracing model used for this comparison (RAYCUB) was developed by Ondet and Barbry;[19] modifications were made to predict echograms and acoustical parameters, and to account for diffuse reflections as described by Kuttruff.[20] RAYCUB allows the user to input relevant room characteristics (room dimensions, source/receiver positions, absorption coefficients, air-absorption exponents). Also input are the size of the receiver (a cube of finite volume), the number of rays to be traced, the number of ray trajectories, and the sampling rate (fixing the echogram time-bin size), as well as a seed number (to initialize the random number generator). To account for diffuse reflection, two random numbers are selected to determine the direction of the reflected ray. The first number is chosen in the interval $(-\pi,\pi)$ to define the azimuthal angle of the reflected ray. The polar angle of the reflected ray is defined by the arccosine of the square root of the second number, chosen in the interval (0,1). Details about this method can be found in Kuttruff.[20]

B. Comparisons

The ray-tracing model was used to predict the echograms for the four cubic rooms. To ensure high preci-

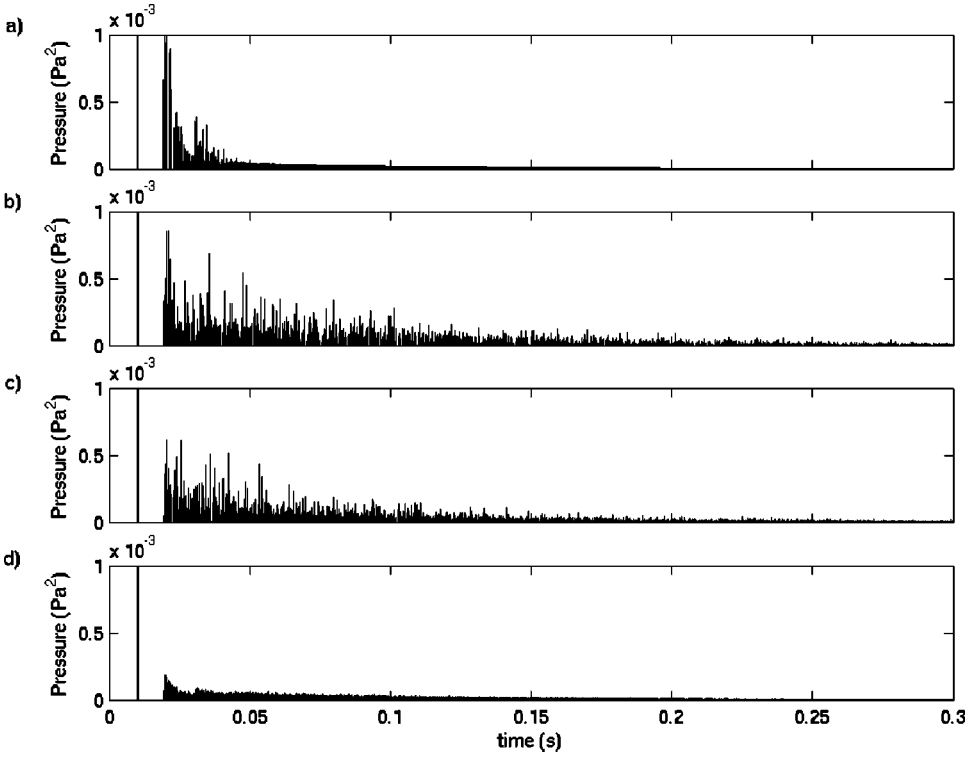


FIG. 6. Echograms for cube 1 predicted by (a) radiosity; (b) ray tracing with 1 million rays; (c) ray tracing with 50 million rays; (d) ray tracing with 1 million rays averaged over 64 runs. Radiosity: 600 patches, $\Delta t = 1/24\,000$, $t_{\text{exact}} = 0.8$ s, and $t_{\text{final}} = 1.0$ s. Ray tracing: diffuse reflection, 500 reflections, 24 kHz, $(0.1\text{ m})^3$ receiver. Range reduced to cut off the direct signal to show detail.

sion, a million rays were traced for 500 reflections at a sampling frequency of 24 kHz. The receiver was a cubic cell with side lengths of 0.1 m.

Echograms obtained by radiosity (with 600 patches and $\Delta t = 1/24\,000$) and ray tracing for cube 1 are shown in Figs. 6(a) and 6(b) (echograms for the other cubes are similar). The echograms are clearly quite different; the echogram for ray tracing has more peaks than the radiosity echogram. It seems that radiosity smears the energy in time more than ray tracing with diffuse reflection.

When the discretized echograms are compared, small differences in the distribution of energy is apparent for all cubes (Fig. 7 shows the discretized echogram for cube 3—the other cubes showed similar trends). In general, it can be observed that total energy levels are higher for radiosity in very early time steps (before 200 ms), and that levels become more similar in later time steps. This suggests, as did observation of the echograms, that radiosity tends to smear (or diffuse) energy faster than ray tracing with diffuse reflection.

Values of the parameter predictions for the cubes are given in Table VII(a). In general, ray tracing with diffuse reflection gives predictions quite similar to predictions by radiosity (see Table III). The parameter that exhibits the greatest difference between predictions is C_{80}; differences for these parameters never exceed 16%. RT, EDT, TS, and D_{50} predictions are all within 8%. Radiosity predictions for L_p are all within 2% of ray-tracing predictions. Note that, for the cubic enclosures, ray-tracing predictions of L_p are consistently lower than predictions by radiosity.

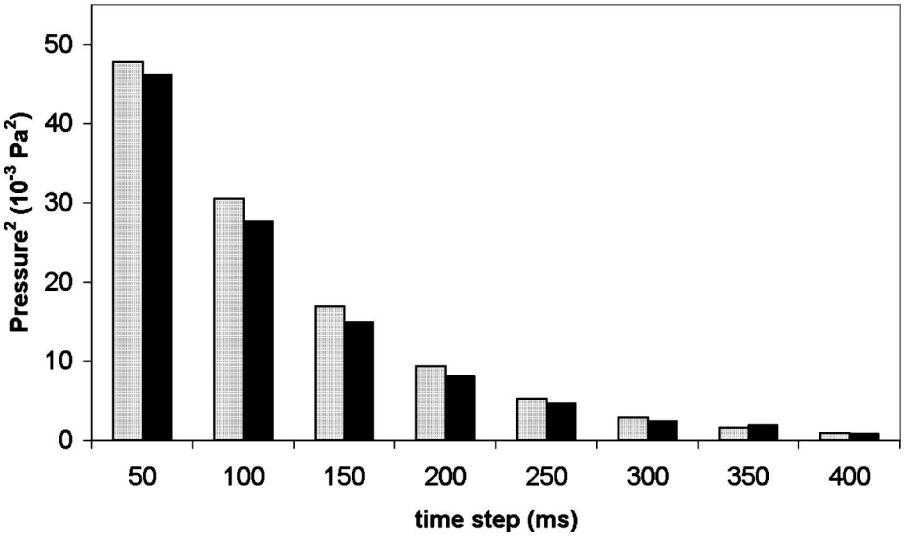


FIG. 7. Discretized echograms with time resolution of 0.05 s for cube 3 predicted by radiosity (600 patches, $\Delta t = 1/24\,000$, $t_{\text{exact}} = 0.8$ s, and $t_{\text{final}} = 1.0$ s) and ray tracing (1 million rays).

TABLE VII. Parameter predictions by ray tracing for the four cubic rooms with (a) 1 million rays; (b) 50 million rays; (c) average over 64 runs with 1 million rays [diffuse reflection, 500 reflections, 24 kHz, $(0.1\ \mathrm{m})^3$ receiver].

	Cube	L_p (dB)	C_{80} (dB)	D_{50} (%)	EDT (s)	RT (s)	TS (ms)
(a)	1	84.58	2.15	46.23	1.21	1.24	92.89
	2	83.29	2.45	46.41	1.03	1.09	86.41
	3	83.95	2.24	47.97	1.26	1.18	92.91
	4	83.86	2.31	46.46	1.15	1.13	91.82
(b)	1	84.57	1.98	46.89	1.22	1.22	93.71
(c)	1	84.57	2.02	45.87	1.22	1.23	94.50
	2	83.45	2.83	49.69	1.13	0.98	84.95
	3	84.31	2.31	46.24	1.18	1.16	91.38
	4	83.84	2.24	46.80	1.18	1.18	91.31

C. Discussion

The differences in the predictions of the parameters, echograms, and discretized echograms for radiosity and ray tracing with diffuse reflection are likely a consequence of the different manner in which diffuse reflection is incorporated in the models. Indeed, a diffusely reflected ray in RAYCUB is not scattered in all directions (as it is in radiosity) but only in one random direction. Consequently, the energy of the ray is not broken into many parts. Rays with high amounts of energy retain the energy, resulting in peaks in the echogram and less smearing of energy. In radiosity, all energy is immediately scattered, so that no larger ''bundles'' of energy remain intact to propagate through the system to cause peaks in the echogram. Also, because of this scattering in radiosity, energy is quickly smeared in time, giving different discretized echograms and parameter predictions.

Still, in the limiting cases (with infinitely many rays traced indefinitely with a point receiver in ray tracing, and with infinitely many patches and continuous time in radiosity) the two methods should be equivalent.[9] It was, therefore, surprising to find such big differences, particularly in the echograms (where the difference is most pronounced). Several attempts were made to investigate this, including performing further predictions with finer meshing of the room surfaces in radiosity, and further predictions with ray tracing. Increasing the number of patches did not improve the comparison but, as the number of rays increased in ray tracing, the echograms became more similar. Echograms from a simulation for cube 1 with 50 million rays is shown in Fig. 6(c), and parameter predictions for cube 1 are given in Table VII(b).

To check for noise artifacts in ray tracing, which could be the source of the problem, the number of rays hitting the receiver in the ray-tracing simulations was recorded. It was approximately 18 000 for 1 million rays, 178 860 for a run with 10 million rays, and 902 014 for 50 million rays. Indeed, the number of hits increased linearly with the number of rays. When the ray-tracing model was run again with different initialization numbers, the echograms were different, indicating that the solution may not have converged. Certainly, the echogram for the case of 50 million rays looks more similar to the radiosity echogram than that for the case of 1 million rays—some of the most predominant peaks were reduced in amplitude. Still, it cannot be concluded that the two methods give similar echograms. Predicted discretized echograms also changed with increasing numbers of rays, but those for ray tracing with 50 million rays were not obviously closer to radiosity than those with fewer rays. Errors in parameter values did not improve with increasing number of rays.

It would be of interest to run RAYCUB for an even larger number of rays. This could not be done because of time constraints (the run with 10 million rays took 15 h on a Pentium III 500-MHz PC; the one with 50 million rays took 80 h on a Pentium 4 2.2-GHz PC). There is a possibility that, with many more rays, ray tracing would converge to the radiosity solution. If this were the case, then it could be concluded that radiosity presents a more efficient way to predict the details of echograms for rooms with diffuse reflection (the run for radiosity took about 5 h, and only seconds for changing receiver positions once the enclosure was rendered). It may also be the case, however, that, with a much finer meshing, radiosity echogram predictions more closely resemble ray-tracing predictions. Very long run times prohibit an exhaustive investigation of the issue at this time. A possible conclusion is that the presented results may not represent converged solutions, but that they do represent practical limits in the algorithms used and in current computing capabilities.

A second idea was to average many ray-tracing runs, each with a different random initialization number. This was done for all cubes with 1 million rays averaged over 64 runs. The resulting echogram for cube 1 is shown in Fig. 6(d), and parameter predictions are given in Table VII(c). The tail (after about 0.05 s) of the echogram looks more similar to the radiosity echogram than the nonaveraged echogram, but the early part is missing some of the more prominent arrivals that are seen in the radiosity echogram—they have been lost in the averaging process. Parameter predictions are, in general, much closer to radiosity predictions than before. Once again, L_p were consistently lower than predictions by radiosity.

An alternative approach would be to use a ray tracer that incorporates diffuse reflection in a different way. It could, for instance, spawn a hundred or more rays for reflection from each diffuse surface, and assign a portion of the incident ray's energy (according to Lambert's cosine law) to each spawned ray. This approach would likely reduce the noise of the stochastic solution and may give results more similar to the radiosity predictions.

V. CONCLUSION

Several things can be learned from the predictions made for the four cubic ($8\times8\times8$-m) enclosures using the acoustical radiosity algorithms and methods developed in Nosal *et al.*[1] First, the predictions suggest that 150 patches, discretization periods of 1/4000 s, and impulse responses predicted exactly for slightly over half of the total predicted length of the response, where cutoff times are determined by Eq. (1), are sufficient for accurate prediction in these enclosures. Second, different distributions of absorption have a significant effect on the sound fields in enclosures with diffusely reflecting boundaries—more uniform distributions

lead to slower decays (hence longer reverberation times, higher center times, and lower clarities and definitions). Moreover, computational time complexity increases as the square of the number of patches, while memory complexity increases linearly with the number of patches. Both time and memory complexity are inversely proportional to time resolution. Furthermore, estimation of form factors by way of configuration factors (such as those predicted by HELIOSFF) does not significantly affect prediction accuracy. In general, radiosity smears energy in time, and eliminates any strong reflections from the echogram. This may make it insufficient for realistic rendering (auralization) of sound fields, in which strong signals have considerable effect on listener perception.

Although not expected, significant differences between radiosity and diffuse ray-tracing echogram predictions were found. There is reason to believe that the ray-tracing predictions had not converged for 1 million rays, or even for 50 million rays, and that echograms for radiosity and ray tracing would look more similar for converged predictions. Ray-tracing predictions averaged over 64 runs had more similarities in the late decay and in parameter predictions. Limitations of the algorithms, and of current computing capabilities, may be the restrictive factor for a perfect comparison.

Despite the differences in the detailed echograms, the discretized echograms predicted by radiosity are similar to those predicted by ray tracing, as are parameter predictions. In the case of the cubic enclosures considered in this research, these are within 16% for C_{80}, 8% for RT, EDT, TS, and D_{50}, and 2% for L_p.

The question of why radiosity and ray tracing predict different echograms is of immediate interest to future research in acoustical radiosity. Ideally, further simulations would be run, for a sufficiently large number of rays in ray tracing and, possibly, for a very fine meshing of the enclosure for radiosity. In addition, it would be interesting to look further into the conditions for convergence of acoustical radiosity and to do further comparisons to ray tracing—possibly for noncubic, and even nonrectangular enclosures. Beyond this, comparisons of radiosity predictions (and those by ray tracing for various surface-reflection laws) to measurements made in real rooms are needed to validate the methods.

ACKNOWLEDGMENTS

We gratefully acknowledge the Natural Sciences and Engineering Research Council of Canada for financial support, and the Institute of Applied Mathematics at UBC for facilitating collaboration between the authors. Also, many warm thanks to Sander Calisal and Wolfgang Heidrich for their valuable suggestions and input to this work.

[1] E.-M. Nosal, M. R. Hodgson, and I. Ashdown, "Improved algorithms and methods for room sound-field prediction by acoustical radiosity in arbitrary polyhedral rooms," J. Acoust. Soc. Am. **116**(2), 970–980 (2004).
[2] MATLAB is a registered trademark of *The Math Works, Inc.*
[3] J. Kang, "Reverberation in rectangular long enclosures with diffusely reflecting boundaries," Acust. Acta Acust. **88**, 77–87 (2002).
[4] H. Kuttruff, "A simple iteration scheme for the computation of decay constants in enclosures with diffusely reflecting boundaries," J. Acoust. Soc. Am. **98**(1), 288–293 (1995).
[5] H. Kuttruff, "Energetic sound propagation in rooms," Acust. Acta Acust. **83**, 622–628 (1997).
[6] R. N. Miles, "Sound field in a rectangular enclosure with diffusely reflecting boundaries," J. Sound Vib. **92**(2), 203–226 (1984).
[7] J. Shi, A. Zhang, J. Encarnação, and M. Göbel, "A modified radiosity algorithm for integrated visual and auditory rendering," Comput. Graph. **17**(6), 633–642 (1993).
[8] M. R. Schroeder and D. Hackman, "Iterative calculation of reverberation time," Acustica **45**, 269–273 (1980).
[9] A. LeBot and A. Bocquillet, "Comparison of an integral equation on energy and the ray-tracing technique in room acoustics," J. Acoust. Soc. Am. **108**(4), 1732–1740 (2000).
[10] H. Kuttruff, *Room Acoustics*, 4th ed. (Spon, London, 2000).
[11] A. G. Sotiropoulou and D. B. Fleming, "Concert hall acoustic evaluations by ordinary concert-goers. II. Physical room acoustics criteria subjectively significant," Acustica **81**(1), 10–19 (1995).
[12] J. S. Suh and P. A. Nelson, "Measurement of transient response f rooms and comparison with geometrical acoustic models," J. Acoust. Soc. Am. **105**(4), 2304–2317 (1999).
[13] U. Gross, K. Spindler, and E. Hahne, "Shape-factor equations for radiation heat transfer between plane rectangular surfaces of arbitrary position and size with rectangular surfaces of arbitrary position and size with rectangular boundaries," Lett. Heat Mass Transfer **8**, 219–227 (1981).
[14] E.-M. Nosal, "Criteria for impulse response length for accurate reverberation time prediction," J. Acoust. Soc. Am. (submitted).
[15] M. R. Hodgson, "When is diffuse-field theory applicable," Appl. Acoust. **49**(3), 197–207 (1996).
[16] G. J. Etgen, *Salas and Hille's Calculus—Several Variables*, 7th ed. (Wiley, New York, 1995).
[17] J. H. Ferziger, *Numerical Methods for Engineering Application*, 2nd ed. (Wiley Interscience, New York, 1998).
[18] HELIOSFF is a trademark of *by Heart Consultants Limited* ⟨www.helios32.com⟩.
[19] A. M. Ondet and J. L. Barbry, "Modeling of sound propagation in fitted workshops using ray tracing," J. Acoust. Soc. Am. **85**(2), 787–796 (1989).
[20] H. Kuttruff, "Simulierte Nachhallkurven in Rechteckräumen mit diffusem Schallfeld," [Simulated reverberation curves in rectangular rooms with diffuse sound fields], Acustica **25**(6), 333–342 (1971).